Active Refrigerators Powered by Inertia

Lukas Hecht,[1] Suvendu Mandal,[1] Hartmut Löwen,[2] and Benno Liebchen[1,*]
[1]Institut für Physik kondensierter Materie, Technische Universität Darmstadt, Hochschulstraße 8, D-64289 Darmstadt, Germany
[2]Institut für Theoretische Physik II—Soft Matter, Heinrich-Heine-Universität Düsseldorf, Universitätsstraße 1, D-40225 Düsseldorf, Germany

(Received 17 December 2021; revised 9 May 2022; accepted 14 September 2022; published 18 October 2022)

We present the operational principle for a refrigerator that uses inertial effects in active Brownian particles to locally reduce their (kinetic) temperature by 2 orders of magnitude below the environmental temperature. This principle exploits the peculiar but so-far unknown shape of the phase diagram of inertial active Brownian particles to initiate motility-induced phase separation in the targeted cooling regime only. Remarkably, active refrigerators operate without requiring isolating walls opening the route toward using them to systematically absorb and trap, e.g., toxic substances from the environment.

DOI: 10.1103/PhysRevLett.129.178001

Introduction.—Many processes in nature allow one to readily heat up an isolated system. Examples include the release of heat in chemical reactions occurring, e.g., when burning wood or gas, inelastic collisions occurring within resistors when exposed to electric currents, and mass-energy conversion processes in nuclear power plants and helium-burning stars. Following the second law of thermodynamics, none of these processes can be reverted, making us believe that it is impossible to cool down an isolated physical system. Accordingly, cooling down a target domain such as the inside of a refrigerator or atoms in a magneto-optical trap requires that the relevant domain is in contact with an external bath to which heat can be transferred via conduction, convection, radiation, or evaporation. Accordingly, developing sophisticated techniques to transfer heat from a target system to the environment has been a great challenge of 20th century physics [1–5].

For active systems [6–13], which consist of self-propelled particles and are intrinsically out of equilibrium, the second law does not apply to the active particles (but only to the overall system) [14]. Therefore, in the present Letter, we ask if it is possible to cool down a system of active Brownian particles (ABPs) [6,53] in a certain target region [refrigerator, Fig. 1(a)] in terms of their kinetic temperature [14] without requiring a mechanism to transfer energy to particles in the (spatially separated) environment.

To achieve this, we exploit the previous finding that ABPs can spontaneously phase separate into a dense and a dilute phase [motility-induced phase separation (MIPS)] [7,54–73]. While MIPS behaves similar to an equilibrium phase transition at large scales in the overdamped limit [59,63,73,74], in the presence of inertia, as relevant for, e.g., activated dusty plasmas [75,76] or vibrating granular particles [77–86], the coexisting phases feature different temperatures, which is, in contrast to clustering in granular gases caused by inelastic collisions [87–91], a consequence of self-propulsion and elastic collisions [92,93]. However, this finding alone is not sufficient to design an active refrigerator because it leads to a dense and cold phase, which occurs as randomly distributed clusters that move, merge, and coarsen and ultimately lead to a uniform temperature profile when averaging over many realizations or a long time [Fig. 2(a)].

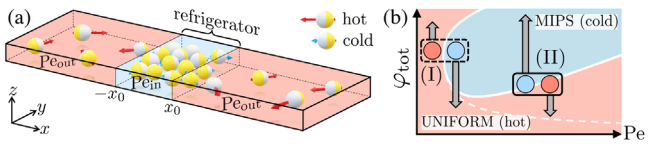

FIG. 1. Schematic of the active refrigerator (a), which exploits the peculiar shape of the phase diagram (b). The blue region represents phase coexistence (MIPS), and the white solid line represents the newly discovered transition line for inertial ABPs in comparison with the well-known transition line for overdamped ABPs (dashed line). Boxes and arrows refer to relevant parameter regimes discussed in the text.

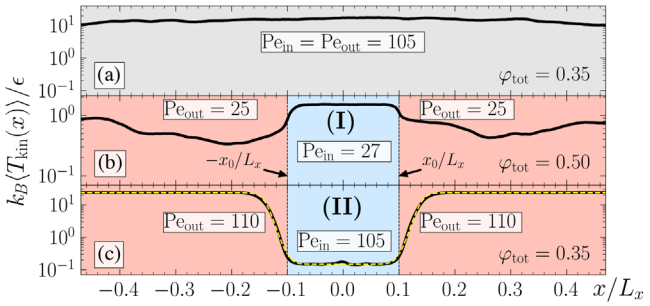

FIG. 2. Kinetic temperature profiles $k_B T_{\mathrm{kin}}(x) = m\langle|\vec{v}|^2\rangle_y/2$ in the steady state averaged over the y coordinate and 20 realizations with $N = 16\,000$ particles for (a) uniform Pe and (b),(c) nonuniform Pe and parameters shown in the key. The yellow dashed line is a fit of $f(x) = a\{2 - \tanh[b(x+c)] + \tanh[b(x-c)]\}/2 + d$.

Thus, to create an active refrigerator, we need to meet the challenge of finding a mechanism allowing us to initiate MIPS in the targeted cooling domain only and to localize the dense phase in that region. To achieve this, one naive approach could be to implement a nonuniform motility [94,95] (e.g., through controlling the laser intensity in light-fueled swimmers [96–99]) such that particles in the targeted cooling domain show a (large) Péclet number [(Pe) relative importance of self-propulsion compared to diffusion] beyond the critical one for the MIPS phase transition, whereas particles in the environment feature a (small) subcritical Pe [Fig. 1(b), regime (I)]. However, this does not work because Pe and the density essentially behave inversely to each other [7,60] such that locally increasing Pe decreases the density in the same spatial region and does not result in a significant temperature difference [Fig. 2(b)]. Remarkably, however, the opposite strategy turns out to work in a carefully selected portion of the phase diagram [Fig. 1(b), regime (II)]: we find that reducing Pe in the targeted cooling domain by less than 5% as compared to the environment reduces the kinetic temperature of the ABPs by 2 orders of magnitude. This surprising finding exploits a remarkable difference between the phase diagram of inertial ABPs and the well-known phase diagram of overdamped ABPs: while MIPS occurs in overdamped ABPs when both Pe and the density are sufficiently large, in underdamped ABPs, it occurs at sufficiently large density and intermediate Pe. Thus, when choosing values of Pe within this intermediate regime in the targeted cooling domain and higher values in the environment, the density further increases in the former region, bringing the system deeper into the MIPS regime and further away from it outside. That is, inertia is required twice: first, to induce the two-temperature coexistence and second, to create the required shape of the phase diagram.

The resulting active refrigerator exemplifies a fundamentally new way to locally cool down a physical system. Like ordinary refrigerators, it can be used to cool down other objects. However, as opposed to ordinary cooling devices, active refrigerators use a self-organized cooling domain such that no isolating walls are required to separate the cooling domain from its environment. As a consequence, active refrigerators can, in principle, also be used as a device to absorb particles from the environment and to store them for a long time, as we shall see.

Model.—We consider inertial active Brownian particles [53,69,72,92,100,101] in two spatial dimensions. Each particle is represented by a (slightly soft) disk of diameter σ, mass m, and moment of inertia $I = m\sigma^2/10$ and features an effective self-propulsion force $\vec{F}_{\mathrm{SP},i} = \gamma_t v_0 \hat{p}_i(t)$, where v_0, $\hat{p}_i$ denote the (terminal) self-propulsion speed and the orientation $\hat{p}_i(t) = (\cos\phi_i(t), \sin\phi_i(t))$ of the ith particle ($i = 1, 2, \ldots, N$), respectively. Position $\vec{r}_i$ and orientation angle ϕ_i evolve according to $d\vec{r}_i/dt = \vec{v}_i$ and $d\phi_i/dt = \omega_i$, respectively, where the velocity $\vec{v}_i$ and the angular velocity ω_i in turn evolve as

$$m\frac{d\vec{v}_i}{dt} = -\gamma_t\vec{v}_i + \gamma_t v_0\hat{p}_i - \sum_{\substack{j=1\\ j\neq i}}^{N}\nabla_{\vec{r}_i}u(r_{ij}) + \sqrt{2k_BT_b\gamma_t}\vec{\xi}_i, \quad (1)$$

$$I\frac{d\omega_i}{dt} = -\gamma_r\omega_i + \sqrt{2k_BT_b\gamma_r}\eta_i. \quad (2)$$

Here, γ_t and γ_r are the translational and rotational drag coefficients, respectively, and T_b is the temperature of the bath, e.g., of the liquid or plasma medium surrounding the particles, which can differ from the kinetic temperature of the particles [102] and which we treat as constant in our simulations (see Supplemental Material [14]). The interaction potential $u(r_{ij})$, $r_{ij} = |\vec{r}_i - \vec{r}_j|$ is modeled by the Weeks-Chandler-Anderson potential [103] with strength ε and effective particle diameter σ. Finally, $\vec{\xi}_i$ and η_i denote Gaussian white noise with zero mean and unit variance. We define $\mathrm{Pe} = v_0/\sqrt{2D_rD_t}$, where $D_t = k_BT_b/\gamma_t$ and $D_r = k_BT_b/\gamma_r$ denote the translational and rotational diffusion coefficients, respectively. Note that ABP models like ours do not explicitly describe the self-propulsion mechanism, the underlying energy source, or how energy is dissipated into the bath [53,104]. We discuss possible experimental realizations below and develop a thermodynamically consistent picture in the paragraph "where does the energy flow?".

In all simulations, we fix $m/(\gamma_t\tau_p) = 5\times10^{-2}$, $I/(\gamma_r\tau_p) = 5\times10^{-3}$, $\varepsilon/(k_BT_b) = 10$, and $\sigma/\sqrt{D_rD_t} = 1$ with the persistence time $\tau_p = 1/D_r$. We choose $\gamma_t = \gamma_r/\sigma^2$ and vary Pe and the total area fraction $\varphi_{\mathrm{tot}} = N\pi\sigma^2/(4A)$, where $A = L_xL_y, L_y/L_x = 0.05$, denotes the area of the simulation box. The Langevin equations are solved numerically with LAMMPS [105,106] for up to $N = 10^5$ particles using periodic boundary conditions and a time step $\Delta t/\tau_p = 10^{-5}$ (see Supplemental Material [14] for further details).

Our setup is illustrated in Fig. 1(a): the simulation area is divided into two regions, in which the particles have different Péclet numbers $\mathrm{Pe}(x_i) = v_0(x_i)/\sqrt{2D_rD_t}$, i.e., the self-propulsion speed of each particle depends on its position according to

$$v_0(x_i) = \begin{cases} v_{0,\mathrm{in}}, & -x_0 < x_i < x_0 \\ v_{0,\mathrm{out}}, & \text{else} \end{cases}, \quad (3)$$

with $x_0 \ll L_x$. Note that our results are robust with respect to changes of x_0, N, m, $v_{0,\mathrm{in}}$, and $v_{0,\mathrm{out}}$ and, in particular, apply to values of $m/(\gamma_t\tau_p)$ used in previous works [70,72,92,93,107,108] (Figs. S9–S12 in the Supplemental Material [14]). Initially, all particles are uniformly distributed in the whole simulation area.

Active refrigerators.—The goal is now to find $\mathrm{Pe}_{\mathrm{in}}$ and $\mathrm{Pe}_{\mathrm{out}}$ such that (i) MIPS occurs in the targeted cooling domain only and (ii) the resulting dense phase stays in that region. Notice first that, when choosing $\mathrm{Pe}_{\mathrm{in}} = \mathrm{Pe}_{\mathrm{out}}$, in each individual realization, we find different kinetic temperatures in coexisting phases, but the ensemble-averaged (or time-averaged) kinetic temperature profile is uniform [Fig. 2(a)]. If we choose $\varphi_{\mathrm{tot}} = 0.5$ and $\mathrm{Pe}_{\mathrm{in}} > \mathrm{Pe}_{\mathrm{out}}$ [regime (I) in Fig. 1(b)] to trigger MIPS in the target domain only, however, we obtain only a weak temperature difference (which even goes in the wrong direction), because the particle density compensates the difference in Pe (because the residential time of a particle in a small volume element scales inversely to its speed) as indicated by the gray arrows in Fig. 1(b) (note that the arrow length depends on the density of both phases and thus is not obvious). More generally, when choosing other combinations $\mathrm{Pe}_{\mathrm{in}} > \mathrm{Pe}_{\mathrm{out}}$ and density in the left part of the phase diagram [Fig. 1(b), regime (I)], we do not observe any relevant cooling in the target domain. Remarkably, however, if we choose a comparatively low area fraction of $\varphi_{\mathrm{tot}} = 0.35$ and $\mathrm{Pe}_{\mathrm{in}} = 105 < \mathrm{Pe}_{\mathrm{out}} = 110$ [regime (II) in Fig. 1(b)], we observe that the system undergoes MIPS exclusively in the target domain and the dense phase remains in that region (Movie M1 in the Supplemental Material [14]). This results in a striking cooling effect by more than 2 orders of magnitude in the cooling domain from $k_B\langle T_{\mathrm{kin}}^{(\mathrm{out})}\rangle/\varepsilon \approx 23.4$ to $k_B\langle T_{\mathrm{kin}}^{(\mathrm{in})}\rangle/\varepsilon \approx 0.147$ [Fig. 2(c)], which is further enhanced when choosing larger Pe differences and complemented by a significantly lower entropy production rate in the cooling domain and an inward flow of kinetic energy (Figs. S3–S5 in the Supplemental Material [14]).

Phase diagram.—To understand the possible parameter choices for constructing active refrigerators in detail, we now discuss the phase diagram of inertial ABPs in the Pe-φ_{tot} plane, which has remained unknown to date. The key control parameters of the system are ε, Pe, and φ_{tot} for fixed m and I. We additionally fix ε and vary Pe and φ_{tot}. To determine the transition line between the uniform state and the MIPS regime (Fig. 3), we investigate the distribution of the local area fraction φ_{loc} [67,72,109], which is unimodal in the uniform regime and bimodal in the coexistence regime (Fig. S1 in the Supplemental Material [14]). Interestingly, the transition line does not follow the well-known relation $\mathrm{Pe} \propto 1/\varphi_{\mathrm{tot}}$, which was found in the overdamped regime [54,56]. In striking contrast, we find that $\mathrm{Pe} \propto \varphi_{\mathrm{tot}}$ in the large Pe regime (green part of the transition line in Fig. 3). This relation serves as a crucial ingredient to construct an active refrigerator. Intuitively, it can be understood to occur as a direct consequence of inertial effects: the particles bounce back when they collide with each other and the rebound is much stronger for large Pe than for moderate Pe. Therefore, to slow down locally, more collisions are necessary and a larger area fraction is required at larger Pe to initiate MIPS.

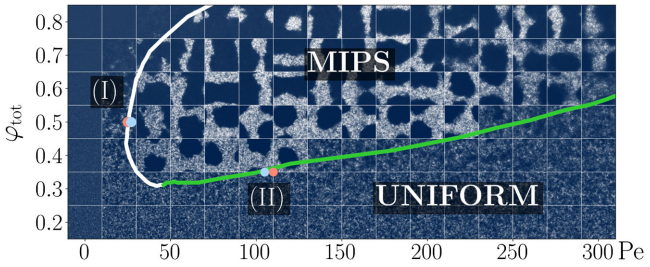

FIG. 3. Phase diagram of $N = 20\,000$ inertial ABPs (background images are steady-state snapshots). The solid line shows the transition line (see Supplemental Material [14] for details). In the vicinity of its green part, parameters can be chosen to construct active refrigerators.

Design rule.—Based on the transition line, we can formulate the following strategy to realize the active refrigerator: first, we want to initiate MIPS in the target domain. This can be achieved by choosing $(\mathrm{Pe}_{\mathrm{in}}, \varphi_{\mathrm{in}})$ inside the MIPS region of the phase diagram for the target domain. Second, we do not want the system to undergo MIPS outside the target domain. Hence, we choose $(\mathrm{Pe}_{\mathrm{out}}, \varphi_{\mathrm{out}})$ outside the coexistence region. Third, we want the particle flux that emerges as a consequence of choosing two different Péclet numbers to bring the system deeper into the coexistence regime within the target domain but further away from it outside. Clearly, based on the obtained detailed knowledge of the phase transition line, the first two criteria can be easily met by fixing a suitable area fraction $\varphi_{\mathrm{in}} = \varphi_{\mathrm{out}} = \varphi_{\mathrm{tot}}$ and choosing two Péclet numbers on both sides of the transition line. However, the third criterion can only be met by choosing parameter combinations in the vicinity of the green marked part of the transition line [regime (II)]. To see this, we will next discuss the particle flux that emerges when choosing two different Péclet numbers.

Supportive and counteracting feedback.—Let us first recall that the mean speed of an ABP decreases with increasing φ_{tot} and increases with increasing Pe (Fig. S2 in the Supplemental Material [14]). Consequently, when we have two regions with different Péclet numbers, a lower density will emerge in the high-Pe region and a larger one in the low-Pe region. Therefore, the gray arrows in Fig. 1(b) always point to lower φ_{tot} at the high-Pe point and vice versa.

In regime (I) and, more generally, in the vicinity of the white part of the transition line in Fig. 3, we need to choose $\mathrm{Pe}_{\mathrm{in}} > \mathrm{Pe}_{\mathrm{critical}} > \mathrm{Pe}_{\mathrm{out}}$ to initiate MIPS in the target domain only. Consequently, the density initially decreases in that region [Fig. 4(a)]. Interestingly, the area fraction in the target domain typically decreases to values below the transition line even for a relatively small Pe difference, which fully prevents MIPS in the target domain.

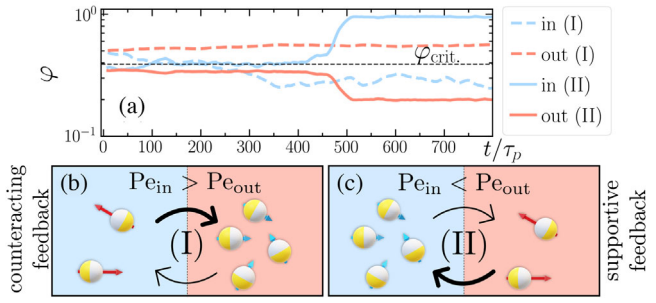

FIG. 4. (a) Area fraction in inner and outer regions over time for regime (I) and (II) (parameters as in Fig. 2). The dashed horizontal line shows the critical area fraction $\varphi_{\text{crit.}} \approx 0.39$ for $\text{Pe} = 27$. A (b) counteracting [(c) supportive] feedback loop decreases [increases] the particle density in the target region.

This surprisingly strong decrease can be viewed as the result of a positive feedback loop [Fig. 4(b)]: the decrease of the particle density in the target domain increases the mean speed of the particles in that region, which further decreases the particle density in the target domain. Thus, no cooling occurs within that region (but rather the opposite, see Fig. 2). In stark contrast, following the peculiar shape of the phase transition line at large Pe (Fig. 3), the initial particle flux points in the right direction and gives rise to the enormous cooling effect for only tiny differences in Pe. More specifically, when choosing $\text{Pe}_{\text{in}} < \text{Pe}_{\text{critical}} < \text{Pe}_{\text{out}}$ [as in regime (II)], the particles are initially faster in the environment, which enhances the density inside the target domain where MIPS occurs and further slows down the particles, which further supports the particle flux from the environment [Fig. 4(c)].

Where does the energy flow?—The finding of a persistent temperature gradient for the active particles is measurable with a suitable thermometer (Supplemental Material [14]) and does, of course, not contradict thermodynamics: heat always flows from hot to cold within the bath (solvent or gas) that surrounds the active particles. This heat flow persists in steady state and is maintained by the (external) energy source driving the system: let us imagine light-powered Janus colloids in a liquid [6] or a complex plasma [75,76], where inertia is important. Clearly, in steady state, when neglecting temperature changes of the particle material, essentially all the energy that is absorbed by the active particles from the external light source is ultimately transferred to the bath. That is, for a uniform Pe (defocused laser), the particles act as identical heat sources for the bath. When realizing active refrigerators with a slightly nonuniform Pe ($\text{Pe}_{\text{out}} \gtrsim \text{Pe}_{\text{in}}$), we obtain a significantly enhanced particle density within the refrigerator region and, hence, a comparatively hot solvent. Thus, T_b is large in regions where T_{kin} is low, leading to a persistent bath energy flow from hot to cold (see Supplemental Material [14] for a minimal model of T_b). Note that changes in T_b are small compared to changes in T_{kin} since the bath has many degrees of freedom. Hence, we keep T_b constant (as typical for ABP models [6]). (This argument is, of course, not restricted to light-powered swimmers but essentially applies also to, e.g., chemically powered swimmers when considering the fuel as an external energy source.)

The direction of the bath energy flow can also be spatially reverted: for $\text{Pe}_{\text{out}} \gg \text{Pe}_{\text{in}}$, the bath heats up stronger outside the refrigerator region because the light absorption grows faster than the particle density inside, which cannot exceed close packing [14]. Then, heat flows into the refrigerator region within the bath but still from hot to cold.

Absorbing, trapping, and cooling tracers with active refrigerators.—One unique feature of the proposed active refrigerators is that they cool down colloidal particles in a certain region in space without requiring any isolating walls separating the cooling domain from the environment. Since the kinetic temperature differences are much larger than the temperature differences in the underlying bath, active refrigerators can also be used to absorb sufficiently large substances from the environment and to trap them for a long time (Fig. 5). To demonstrate this, we have performed simulations of inertial ABPs [parameters as in Fig. 2(c)] and additional passive tracer particles, which may represent, e.g., certain toxic substances and are randomly distributed outside the cooling domain. Remarkably, the active refrigerator systematically absorbs tracers from the environment and cools them by 2 orders of magnitude below the kinetic temperature of tracers outside the refrigerator domain [Fig. 5(a)]. Note that it can take a long time before a tracer enters the cooling domain, but once it is deep inside this region it stays there for a very long time, as indicated by the exemplary trajectories in Fig. 5(b) and Movie M2 in the Supplemental Material [14].

Possible experimental realizations.—Active refrigerators can be realized with self-propelled particles featuring significant inertia and elastic collisions such as activated microparticles in a plasma [75,76], mesoscopic propellers such as vibrated granular particles [77–85], drones [86,110,111], and minirobots [112], and dense animal

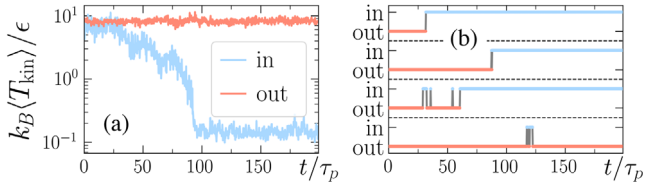

FIG. 5. Absorbing, trapping, and cooling tracers with active refrigerators. (a) Kinetic temperature of passive tracers inside and outside the cooling domain. (b) Position (inside or outside the cooling domain) of four exemplary passive tracers over time [parameters as in Fig. 2(c), but with $\text{Pe}_{\text{in}} = \text{Pe}_{\text{out}} = 0$ for passive tracers and $N_{\text{passive}}/N = 0.02$].

collections [113] such as swimming whirligig beetles, as recently demonstrated in Ref. [114].

Conclusions.—We have proposed a mechanism for an active refrigerator, which requires inertia not only to create a temperature difference across coexisting phases but also to induce the peculiar shape of the MIPS phase transition line, which we exploit to localize the cooling domain in a predefined region of space. As their key feature, active refrigerators create a self-organized cooling domain, in which active particles feature a much lower kinetic temperature compared to their environment. As they do not require any isolating walls to separate the cooling domain from its environment, active refrigerators prove a route toward possible future applications, e.g., to trap and absorb large (toxic) molecules or viruses. Overall, we found that the active-particle subsystem alone does not behave as one might expect from the laws of thermodynamics, but makes the bath pay the thermodynamic bill for a self-organized cooling domain that does not decay. This could be further explored within microscopic theories [115,116].

L. H. gratefully acknowledges the support by the German Academic Scholarship Foundation (Studienstiftung des deutschen Volkes).

*benno.liebchen@pkm.tu-darmstadt.de

[1] H. J. Metcalf and P. van der Straten, *Laser Cooling and Trapping*, Graduate Texts in Contemporary Physics (Springer, New York, 1999).
[2] D. V. Schroeder, *An Introduction to Thermal Physics* (Oxford University Press, Oxford, 2021).
[3] A. Ziabari, M. Zebarjadi, D. Vashaee, and A. Shakouri, Nanoscale solid-state cooling: A review, Rep. Prog. Phys. **79**, 095901 (2016).
[4] V. S. Letokhov, M. A. Ol'shanii, and Y. B. Ovchinnikov, Laser cooling of atoms: A review, Quantum Semiclass. Opt. **7**, 5 (1995).
[5] C. Van den Broeck and R. Kawai, Brownian Refrigerator, Phys. Rev. Lett. **96**, 210601 (2006).
[6] C. Bechinger, R. Di Leonardo, H. Löwen, C. Reichhardt, G. Volpe, and G. Volpe, Active Particles in Complex and Crowded Environments, Rev. Mod. Phys. **88**, 045006 (2016).
[7] M. E. Cates and J. Tailleur, Motility-induced phase separation, Annu. Rev. Condens. Matter Phys. **6**, 219 (2015).
[8] M. C. Marchetti, J. F. Joanny, S. Ramaswamy, T. B. Liverpool, J. Prost, M. Rao, and R. A. Simha, Hydrodynamics of soft active matter, Rev. Mod. Phys. **85**, 1143 (2013).
[9] J. Elgeti, R. G. Winkler, and G. Gompper, Physics of microswimmers—single particle motion and collective behavior: A review, Rep. Prog. Phys. **78**, 056601 (2015).
[10] G. Gompper, R. G. Winkler, T. Speck, A. P. Solon, C. Nardini, F. Peruani, H. Löwen, R. Golestanian, U. B. Kaupp, L. Alvarez *et al.*, The 2020 motile active matter roadmap, J. Phys. Condens. Matter **32**, 193001 (2020).
[11] M. J. Bowick, N. Fakhri, M. C. Marchetti, and S. Ramaswamy, Symmetry, Thermodynamics, and Topology in Active Matter, Phys. Rev. X **12**, 010501 (2022).
[12] B. Liebchen and A. K. Mukhopadhyay, Interactions in active colloids, J. Phys. Condens. Matter **34**, 083002 (2022).
[13] D. Schildknecht, A. N. Popova, J. Stellwagen, and M. Thomson, Reinforcement learning reveals fundamental limits on the mixing of active particles, Soft Matter **18**, 617 (2022).
[14] See Supplemental Material at http://link.aps.org/supplemental/10.1103/PhysRevLett.129.178001 for details about the simulation, the phase diagram, and the swimming speed, a discussion about design parameters, kinetic temperature, entropy production, and heat and energy flow, a minimal model for the bath temperature, and Movies M1 and M2, which includes Refs. [15–52].
[15] V. Ramasubramani, B. D. Dice, E. S. Harper, M. P. Spellings, J. A. Anderson, and S. C. Glotzer, freud: A software suite for high throughput analysis of particle simulation data, Comput. Phys. Commun. **254**, 107275 (2020).
[16] L. F. Cugliandolo, G. Gonnella, and I. Petrelli, Effective temperature in active brownian particles, Fluct. Noise Lett. **18**, 1940008 (2019).
[17] L. Caprini, A. Puglisi, and A. Sarracino, Fluctuation–dissipation relations in active matter systems, Symmetry **13**, 81 (2021).
[18] D. Levis and L. Berthier, From single-particle to collective effective temperatures in an active fluid of self-propelled particles, Europhys. Lett. **111**, 60006 (2015).
[19] G. Szamel, Self-propelled particle in an external potential: Existence of an effective temperature, Phys. Rev. E **90**, 012111 (2014).
[20] D. Loi, S. Mossa, and L. F. Cugliandolo, Effective temperature of active matter, Phys. Rev. E **77**, 051111 (2008).
[21] A. Puglisi, A. Sarracino, and A. Vulpiani, Temperature in and out of equilibrium: A review of concepts, tools and attempts, Phys. Rep. **709–710**, 1 (2017).
[22] É. Fodor, C. Nardini, M. E. Cates, J. Tailleur, P. Visco, and F. van Wijland, How Far from Equilibrium Is Active Matter?, Phys. Rev. Lett. **117**, 038103 (2016).
[23] D. Chaudhuri, Active Brownian particles: Entropy production and fluctuation response, Phys. Rev. E **90**, 022131 (2014).
[24] S. D. Cengio, D. Levis, and I. Pagonabarraga, Fluctuation–dissipation relations in the absence of detailed balance: Formalism and applications to active matter, J. Stat. Mech. (2021) 043201.
[25] U. Seifert, Stochastic thermodynamics, fluctuation theorems and molecular machines, Rep. Prog. Phys. **75**, 126001 (2012).
[26] J. O'Byrne, Y. Kafri, J. Tailleur, and F. van Wijland, Time irreversibility in active matter, from micro to macro, Nat. Rev. Phys. **4**, 167 (2022).
[27] S. Ro, B. Guo, A. Shih, T. V. Phan, R. H. Austin, D. Levine, P. M. Chaikin, and S. Martiniani, arXiv: 2105.12707v3 [Play. Pause. Rewind. Measuring Local Entropy Production and Extractable Work in Active Matter, Phys. Rev. Lett. (to be published)].

[28] S. Shankar and M. C. Marchetti, Hidden entropy production and work fluctuations in an ideal active gas, Phys. Rev. E **98**, 020604(R) (2018).

[29] L. Onsager and S. Machlup, Fluctuations and irreversible processes, Phys. Rev. **91**, 1505 (1953).

[30] G. Szamel, Stochastic thermodynamics for self-propelled particles, Phys. Rev. E **100**, 050603(R) (2019).

[31] P. Pietzonka and U. Seifert, Entropy production of active particles and for particles in active baths, J. Phys. A **51**, 01LT01 (2018).

[32] T. Nemoto, É. Fodor, M. E. Cates, R. L. Jack, and J. Tailleur, Optimizing active work: Dynamical phase transitions, collective motion, and jamming, Phys. Rev. E **99**, 022605 (2019).

[33] F. Cagnetta, F. Corberi, G. Gonnella, and A. Suma, Large Fluctuations and Dynamic Phase Transition in a System of Self-Propelled Particles, Phys. Rev. Lett. **119**, 158002 (2017).

[34] T. GrandPre, K. Klymko, K. K. Mandadapu, and D. T. Limmer, Entropy production fluctuations encode collective behavior in active matter, Phys. Rev. E **103**, 012613 (2021).

[35] N. A. Söker, S. Auschra, V. Holubec, K. Kroy, and F. Cichos, How Activity Landscapes Polarize Microswimmers without Alignment Forces, Phys. Rev. Lett. **126**, 228001 (2021).

[36] S. Auschra, V. Holubec, N. A. Söker, F. Cichos, and K. Kroy, Polarization-density patterns of active particles in motility gradients, Phys. Rev. E **103**, 062601 (2021).

[37] R. Zwanzig, *Nonequilibrium Statistical Mechanics* (Oxford University Press, New York, 2001).

[38] Y. Komatsu and H. Tanaka, Roles of Energy Dissipation in a Liquid-Solid Transition of Out-of-Equilibrium Systems, Phys. Rev. X **5**, 031025 (2015).

[39] J. J. Brey, J. W. Dufty, C. S. Kim, and A. Santos, Hydrodynamics for granular flow at low density, Phys. Rev. E **58**, 4638 (1998).

[40] R. Livi and P. Politi, *Nonequilibrium Statistical Physics* (Cambridge University Press, Cambridge, England, 2017).

[41] R. B. Bird, W. E. Stewart, and E. N. Lightfoot, *Transport Phenomena*, 2nd ed. (John Wiley & Sons, New York, 2002).

[42] G. Lebon, D. Jou, and J. Casas-Vázquez, *Understanding Non-Equilibrium Thermodynamics* (Springer, Berlin, Heidelberg, 2008).

[43] U. D. Jentschura and J. Sapirstein, Green function of the Poisson equation: $D = 2, 3, 4$, J. Phys. Commun. **2**, 015026 (2018).

[44] B. Liebchen and H. Löwen, Modeling chemotaxis of microswimmers: From individual to collective behavior, in *Chemical Kinetics* (World Scientific, Singapore, 2019), p. 493.

[45] K. Cole, J. Beck, A. Haji-Sheikh, and B. Litkouhi, *Heat Conduction Using Greens Functions*, 2nd ed. (CRC Press, Boca Raton, 2010).

[46] E. N. Economou, *Green's Functions in Quantum Physics* (Springer, Berlin, Heidelberg, 2006).

[47] B. Städler, A. D. Price, R. Chandrawati, L. Hosta-Rigau, A. N. Zelikin, and F. Caruso, Polymer hydrogel capsules: en route toward synthetic cellular systems, Nanoscale **1**, 68 (2009).

[48] T. M. S. Chang, Semipermeable microcapsules, Science **146**, 524 (1964).

[49] N. Greinert, T. Wood, and P. Bartlett, Measurement of Effective Temperatures in an Aging Colloidal Glass, Phys. Rev. Lett. **97**, 265702 (2006).

[50] S. Ye, P. Liu, F. Ye, K. Chen, and M. Yang, Active noise experienced by a passive particle trapped in an active bath, Soft Matter **16**, 4655 (2020).

[51] V. Démery and É. Fodor, Driven probe under harmonic confinement in a colloidal bath, J. Stat. Mech. (2019) 033202.

[52] C. Maggi, M. Paoluzzi, N. Pellicciotta, A. Lepore, L. Angelani, and R. Di Leonardo, Generalized Energy Equipartition in Harmonic Oscillators Driven by Active Baths, Phys. Rev. Lett. **113**, 238303 (2014).

[53] P. Romanczuk, M. Bär, W. Ebeling, B. Lindner, and L. Schimansky-Geier, Active Brownian particles, Eur. Phys. J. Special Topics **202**, 1 (2012).

[54] J. Tailleur and M. E. Cates, Statistical Mechanics of Interacting Run-and-Tumble Bacteria, Phys. Rev. Lett. **100**, 218103 (2008).

[55] Y. Fily and M. C. Marchetti, Athermal Phase Separation of Self-Propelled Particles with No Alignment, Phys. Rev. Lett. **108**, 235702 (2012).

[56] M. E. Cates and J. Tailleur, When are active Brownian particles and run-and-tumble particles equivalent? Consequences for motility-induced phase separation, Europhys. Lett. **101**, 20010 (2013).

[57] I. Buttinoni, J. Bialké, F. Kümmel, H. Löwen, C. Bechinger, and T. Speck, Dynamical Clustering and Phase Separation in Suspensions of Self-Propelled Colloidal Particles, Phys. Rev. Lett. **110**, 238301 (2013).

[58] J. Stenhammar, A. Tiribocchi, R. J. Allen, D. Marenduzzo, and M. E. Cates, Continuum Theory of Phase Separation Kinetics for Active Brownian Particles, Phys. Rev. Lett. **111**, 145702 (2013).

[59] G. S. Redner, M. F. Hagan, and A. Baskaran, Structure and Dynamics of a Phase-Separating Active Colloidal Fluid, Phys. Rev. Lett. **110**, 055701 (2013).

[60] J. Stenhammar, D. Marenduzzo, R. J. Allen, and M. E. Cates, Phase behaviour of active Brownian particles: the role of dimensionality, Soft Matter **10**, 1489 (2014).

[61] Z. Mokhtari, T. Aspelmeier, and A. Zippelius, Collective rotations of active particles interacting with obstacles, Europhys. Lett. **120**, 14001 (2017).

[62] A. Patch, D. Yllanes, and M. C. Marchetti, Kinetics of motility-induced phase separation and swim pressure, Phys. Rev. E **95**, 012601 (2017).

[63] D. Levis, J. Codina, and I. Pagonabarraga, Active Brownian equation of state: metastability and phase coexistence, Soft Matter **13**, 8113 (2017).

[64] J. T. Siebert, F. Dittrich, F. Schmid, K. Binder, T. Speck, and P. Virnau, Critical behavior of active Brownian particles, Phys. Rev. E **98**, 030601(R) (2018).

[65] A. P. Solon, J. Stenhammar, M. E. Cates, Y. Kafri, and J. Tailleur, Generalized thermodynamics of motility-induced phase separation: Phase equilibria, Laplace pressure, and change of ensembles, New J. Phys. **20**, 075001 (2018).

[66] M. Durve, A. Saha, and A. Sayeed, Active particle condensation by non-reciprocal and time-delayed interactions, Eur. Phys. J. E **41**, 49 (2018).
[67] P. Digregorio, D. Levis, A. Suma, L. F. Cugliandolo, G. Gonnella, and I. Pagonabarraga, Full Phase Diagram of Active Brownian Disks: From Melting to Motility-Induced Phase Separation, Phys. Rev. Lett. **121**, 098003 (2018).
[68] A. Patch, D. M. Sussman, D. Yllanes, and M. C. Marchetti, Curvature-dependent tension and tangential flows at the interface of motility-induced phases, Soft Matter **14**, 7435 (2018).
[69] H. Löwen, Inertial effects of self-propelled particles: From active Brownian to active Langevin motion, J. Chem. Phys. **152**, 040901 (2020).
[70] C. Dai, I. R. Bruss, and S. C. Glotzer, Phase separation and state oscillation of active inertial particles, Soft Matter **16**, 2847 (2020).
[71] S. Chennakesavalu and G. M. Rotskoff, Probing the theoretical and computational limits of dissipative design, J. Chem. Phys. **155**, 194114 (2021).
[72] J. Su, H. Jiang, and Z. Hou, Inertia-induced nucleation-like motility-induced phase separation, New J. Phys. **23**, 013005 (2021).
[73] F. Turci and N. B. Wilding, Phase Separation and Multibody Effects in Three-Dimensional Active Brownian Particles, Phys. Rev. Lett. **126**, 038002 (2021).
[74] J. O'Byrne and J. Tailleur, Lamellar to Micellar Phases and Beyond: When Tactic Active Systems Admit Free Energy Functionals, Phys. Rev. Lett. **125**, 208003 (2020).
[75] G. E. Morfill and A. V. Ivlev, Complex plasmas: An interdisciplinary research field, Rev. Mod. Phys. **81**, 1353 (2009).
[76] V. Nosenko, F. Luoni, A. Kaouk, M. Rubin-Zuzic, and H. Thomas, Active Janus particles in a complex plasma, Phys. Rev. Res. **2**, 033226 (2020).
[77] C. Scholz, S. Jahanshahi, A. Ldov, and H. Löwen, Inertial delay of self-propelled particles, Nat. Commun. **9**, 5156 (2018).
[78] C. Scholz, S. D'Silva, and T. Pöschel, Ratcheting and tumbling motion of Vibrots, New J. Phys. **18**, 123001 (2016).
[79] A. Kudrolli, G. Lumay, D. Volfson, and L. S. Tsimring Swarming and Swirling in Self-Propelled Polar Granular Rods, Phys. Rev. Lett. **100**, 058001 (2008).
[80] C. A. Weber, T. Hanke, J. Deseigne, S. Léonard, O. Dauchot, E. Frey, and H. Chaté, Long-Range Ordering of Vibrated Polar Disks, Phys. Rev. Lett. **110**, 208001 (2013).
[81] L. Walsh, C. G. Wagner, S. Schlossberg, C. Olson, A. Baskaran, and N. Menon, Noise and diffusion of a vibrated self-propelled granular particle, Soft Matter **13**, 8964 (2017).
[82] G. A. Patterson, P. I. Fierens, F. Sangiuliano Jimka, P. G. König, A. Garcimartín, I. Zuriguel, L. A. Pugnaloni, and D. R. Parisi, Clogging Transition of Vibration-Driven Vehicles Passing through Constrictions, Phys. Rev. Lett. **119**, 248301 (2017).
[83] A. Deblais, T. Barois, T. Guerin, P. H. Delville, R. Vaudaine, J. S. Lintuvuori, J. F. Boudet, J. C. Baret, and H. Kellay, Boundaries Control Collective Dynamics of Inertial Self-Propelled Robots, Phys. Rev. Lett. **120**, 188002 (2018).
[84] L. Giomi, N. Hawley-Weld, and L. Mahadevan, Swarming, swirling and stasis in sequestered bristle-bots, Proc. R. Soc. A **469**, 20120637 (2013).
[85] O. Dauchot and V. Démery, Dynamics of a Self-Propelled Particle in a Harmonic Trap, Phys. Rev. Lett. **122**, 068002 (2019).
[86] J. Deseigne, O. Dauchot, and H. Chaté, Collective Motion of Vibrated Polar Disks, Phys. Rev. Lett. **105**, 098001 (2010).
[87] I. Goldhirsch and G. Zanetti, Clustering instability in dissipative gases, Phys. Rev. Lett. **70**, 1619 (1993).
[88] D. Paolotti, A. Barrat, U. Marini Bettolo Marconi, and A. Puglisi, Thermal convection in monodisperse and bidisperse granular gases: A simulation study, Phys. Rev. E **69**, 061304 (2004).
[89] V. Garzó, A. Santos, and G. M. Kremer, Impact of roughness on the instability of a free-cooling granular gas, Phys. Rev. E **97**, 052901 (2018).
[90] W. D. Fullmer and C. M. Hrenya, The clustering instability in rapid granular and gas-solid flows, Annu. Rev. Fluid Mech. **49**, 485 (2017).
[91] A. Puglisi, V. Loreto, U. M. B. Marconi, A. Petri, and A. Vulpiani, Clustering and Non-Gaussian Behavior in Granular Matter, Phys. Rev. Lett. **81**, 3848 (1998).
[92] S. Mandal, B. Liebchen, and H. Löwen, Motility-Induced Temperature Difference in Coexisting Phases, Phys. Rev. Lett. **123**, 228001 (2019).
[93] I. Petrelli, L. F. Cugliandolo, G. Gonnella, and A. Suma, Effective temperatures in inhomogeneous passive and active bidimensional Brownian particle systems, Phys. Rev. E **102**, 012609 (2020).
[94] C. Lozano, B. Ten Hagen, H. Löwen, and C. Bechinger, Phototaxis of synthetic microswimmers in optical landscapes, Nat. Commun. **7**, 12828 (2016).
[95] C. Lozano, B. Liebchen, B. Ten Hagen, C. Bechinger, and H. Löwen, Propagating density spikes in light-powered motility-ratchets, Soft Matter **15**, 5185 (2019).
[96] M. Heidari, A. Bregulla, S. M. Landin, F. Cichos, and R. von Klitzing, Self-Propulsion of Janus Particles near a Brush-Functionalized Substrate, Langmuir **36**, 7775 (2020).
[97] R. Golestanian, Collective Behavior of Thermally Active Colloids, Phys. Rev. Lett. **108**, 038303 (2012).
[98] H.-R. Jiang, N. Yoshinaga, and M. Sano, Active Motion of a Janus Particle by Self-Thermophoresis in a Defocused Laser Beam, Phys. Rev. Lett. **105**, 268302 (2010).
[99] I. Buttinoni, G. Volpe, F. Kümmel, G. Volpe, and C. Bechinger, Active Brownian motion tunable by light, J. Phys. Condens. Matter **24**, 284129 (2012).
[100] L. L. Gutierrez-Martinez and M. Sandoval, Inertial effects on trapped active matter, J. Chem. Phys. **153**, 044906 (2020).
[101] M. Sandoval, Pressure and diffusion of active matter with inertia, Phys. Rev. E **101**, 012606 (2020).
[102] G. Falasco, M. V. Gnann, D. Rings, and K. Kroy, Effective temperatures of hot Brownian motion, Phys. Rev. E **90**, 032131 (2014).

[103] J. D. Weeks, D. Chandler, and H. C. Andersen, Role of repulsive forces in determining the equilibrium structure of simple liquids, J. Chem. Phys. **54**, 5237 (1971).
[104] L. Hecht, J. C. Ureña, and B. Liebchen, An Introduction to Modeling Approaches of Active Matter, arXiv:2102.13007.
[105] S. Plimpton, Fast parallel algorithms for short-range molecular dynamics, J. Comput. Phys. **117**, 1 (1995).
[106] A. P. Thompson, H. M. Aktulga, R. Berger, D. S. Bolintineanu, W. M. Brown, P. S. Crozier, P. J. in 't Veld, A. Kohlmeyer, S. G. Moore, T. D. Nguyen *et al.*, LAMMPS - a flexible simulation tool for particle-based materials modeling at the atomic, meso, and continuum scales, Comput. Phys. Commun. **271**, 108171 (2022).
[107] L. Caprini and U. Marini Bettolo Marconi, Spatial velocity correlations in inertial systems of active Brownian particles, Soft Matter **17**, 4109 (2021).
[108] S. C. Takatori and J. F. Brady, Inertial effects on the stress generation of active fluids, Phys. Rev. Fluids **2**, 094305 (2017).
[109] J. U. Klamser, S. C. Kapfer, and W. Krauth, Thermodynamic phases in two-dimensional active matter, Nat. Commun. **9**, 5045 (2018).
[110] G. Vásárhelyi, C. Virágh, G. Somorjai, T. Nepusz, A. E. Eiben, and T. Vicsek, Optimized flocking of autonomous drones in confined environments, Sci. Robot. **3**, eaat3536 (2018).
[111] M. Duarte, S. Oliveira, and A. Christensen, Hybrid control for large swarms of aquatic drones, in *Artificial Life 14: Proceedings of the Fourteenth International Conference on the Synthesis and Simulation of Living Systems* (MIT Press, Manhattan, New York, 2014), p. 785.
[112] M. Leyman, F. Ogemark, J. Wehr, and G. Volpe, Tuning phototactic robots with sensorial delays, Phys. Rev. E **98**, 052606 (2018).
[113] D. Klotsa, As above, so below, and also in between: mesoscale active matter in fluids, Soft Matter **15**, 8946 (2019).
[114] H. L. Devereux, C. R. Twomey, M. S. Turner, and S. Thutupalli, Whirligig beetles as corralled active Brownian particles, J. R. Soc. Interface **18**, 20210114 (2021).
[115] D. Arold and M. Schmiedeberg, Mean field approach of dynamical pattern formation in underdamped active matter with short-ranged alignment and distant anti-alignment interactions, J. Phys. Condens. Matter **32**, 315403 (2020).
[116] U. Marini Bettolo Marconi, L. Caprini, and A. Puglisi, Hydrodynamics of simple active liquids: the emergence of velocity correlations, New J. Phys. **23**, 103024 (2021).